Uncertainty Analysis of Coaxial Thermocouple Calorimeters used in Arc Jets

David M. Driver[1], Daniel Philippidis[2], and Imelda Terrazas-Salinas[3]
NASA Ames Research Center, Moffett Field, California, 94035

Recent introduction of Coaxial Thermocouple type calorimeters into the NASA Ames arc jet facilities has inspired an analysis of 2D conduction effects internal to this type of calorimeter. Lateral conduction effects violate the 1D finite slab inverse analysis which is typically used to deduce the heat transfer to such calorimeters. The spherical shaped nose associated with most calorimeters (rather than flat) leads to a bias error that over-estimates the stagnation heating. Non-uniform heating on the face of spherically shaped calorimeters leads to conduction losses to the colder rim of the calorimeter which causes an under-estimate of the stagnation heating. These two effects come into play at different times of the calorimeter's exposure to the arc jet, so they do not cancel. The spherical body effects come into play in the early stages of exposure, while the non-uniform heating effect becomes most severe at the later stages of exposure. The bias associated with spherical effects can be avoided by rewriting the 1D finite slab inverse analysis code to solve for 1D conduction in spherical coordinates. However, reducing the bias error associated non-uniform heating requires a somewhat ad hoc modification to the 1D finite element inverse analysis.

Nomenclature

C_p	=	Heat capacity of the material, J/K-kg
H_r	=	Recovery enthalpy, MJ/kg
k	=	Thermal conductivity of the material, W/m-K
L	=	Thickness of spherical shell, m
M	=	Mach number
p	=	Pressure, Pa
q	=	Heat flux, W/cm^2
r	=	Radial distance from the centerline of the jet, m
R	=	Radial distance from the center of the sphere, m
R_o	=	Radius of curvature of the nose of the model, m
T	=	Temperature, K
t	=	Time since the start of exposure to the arc heated flow, s
x	=	Axial distance from nose tip of calorimeter (in-depth direction is positive x), m
ρ	=	Axial distance from nose tip of calorimeter (in-depth direction is positive x), m

I. Introduction

Arc jet flow characterization is part of an ongoing effort to improve testing and analysis at NASA Ames Research Center. New measurement techniques are routinely being pursued in the interest of reliably obtaining the most accurate measurements possible. Copper slug calorimeters [1] have been the main-stay of stagnation heat flux measurements for the last several decades (see Fig. 1). From an accuracy point of view, there are concerns about the conduction losses through the ruby balls used to hold the slug in place, and the unknown convection effects through the gap between the slug and its holder. Operationally, the main limitation of the slug calorimeter is the need to dwell in the flow for a sufficient period of time to get a steady state measurement, while getting it in and

[1] Senior Research Scientist, Aerothermodynamics Branch, MS 230-2, Associate Fellow AIAA
[2] Engineer, Aerospace Computing Inc., MS 229-4
[3] Test Engineer Thermophysics Facilities Branch, MS 242-2

out of the flow quickly enough so as not to melt the slug. The temperature is measured at the back side of the slug so it is slow to respond to changes in heat flux and is not suitable for making heat flux surveys of the jet.

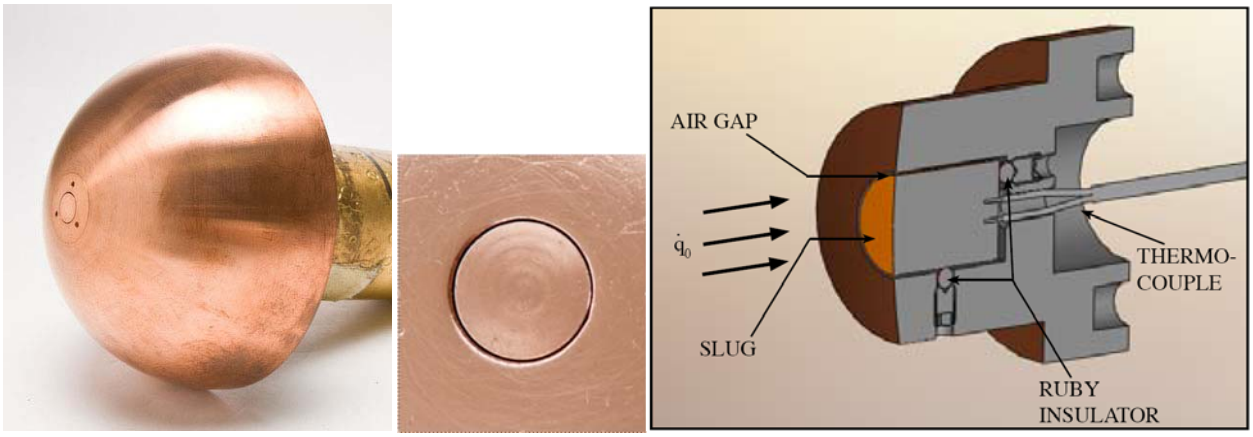

Fig. 1 Slug Calorimeter mounted in a 101.6 mm diameter Hemispherical probe showing the mounting details.

The desire to obtain radial distributions of heat flux (flow field surveys) has led to a continual search for other means of measuring heat transfer. Gardon gauges [2] are periodically considered, but their heavy dependence on calibration and the associated uncertainty has limited their use.

Front surface temperature measurement sensors such as Null Point [3] and Coaxial thermocouple (TC) [4] sensors are attractive alternatives (to the slug) because the sensors respond nearly instantaneously with changes in heat flux, making them a good choice for heat flux surveys of the jet. Null points were adopted in 2007 to deduce radial variations in total enthalpy across the jet (deduced from heat flux survey). The Null points were relied on to give relative measures of the heat flux, while absolute values of heat flux were largely obtained with slug calorimeters. Coaxial TC's were ruled out due to the limitation of materials used at the time – steel, Chromel, which have low thermal diffusivity and low catalytic recombination coefficients.

Coaxial TC sensors were revisited when a Copper-Constantan version of the coaxial thermocouple [5] became available (high thermal diffusivity and relatively high catalytic efficiency). The sensing element is coated with a thin (~18 μm) copper layer (vapor deposited) which is used to complete the thermocouple circuit. The Null point calorimeter measures the temperature ~500μm below the surface at the bottom of a blind hole in the backside of the Null point body – the depth and diameter of the hole are optimized to allow the backside TC to mimic the front side temperature (see ASTM standard ref. [3]). For both devices (coaxial TC and Null point), the determination of surface heat flux from the thermocouple time history is straight forward using the 1D finite slab inverse analysis algorithm [6]. The coaxial TC sensing element was thought be the more accurate of the two by virtue of the thermocouple truly being at the surface and secondly avoidance of a backside cavity. This Copper-Constantan version of coaxial TC sensor, has become so attractive that it is being considered more seriously as the primary measurement of stagnation heat flux in the NASA Ames arc jets. The main downside of the coaxial thermocouple sensor, at least conceptually, is the potential for lateral heat conduction effects, which would violate the assumptions in the 1D finite slab inverse analysis.

No ASTM standard currently exists for coaxial thermocouples. The closest thing to an ASTM standard is the ASTM standard for Null points [3] which describes the 1D finite slab inverse analysis for deducing heat flux from surface temperature measurements – commonly used for both devices. The Null point ASTM standard does not consider lateral conduction effects to the calorimeter body. This paper describes an effort to assess the severity 2D conduction effects in calorimeter probes with an embedded coaxial thermocouple sensors.

II. Coaxial Thermocouple Sensor Description

The coaxial thermocouple probes at NASA Ames each employ a Medtherm [5] sensor which was installed by Arnold Engineering Development Center (AEDC) [7] into the calorimeter body. The sensor contains a central pin (or wire) made of Constantan coated with MgO electrical insulation and housed in a copper tube – and the copper outer tube is swaged around the constantan wire (see Fig. 2). The sensor can be purchased in various diameters and lengths, and the coaxial thermocouple sensors used at Ames are 2.54mm (0.100") in diameter and 10.16mm (0.400") in length.

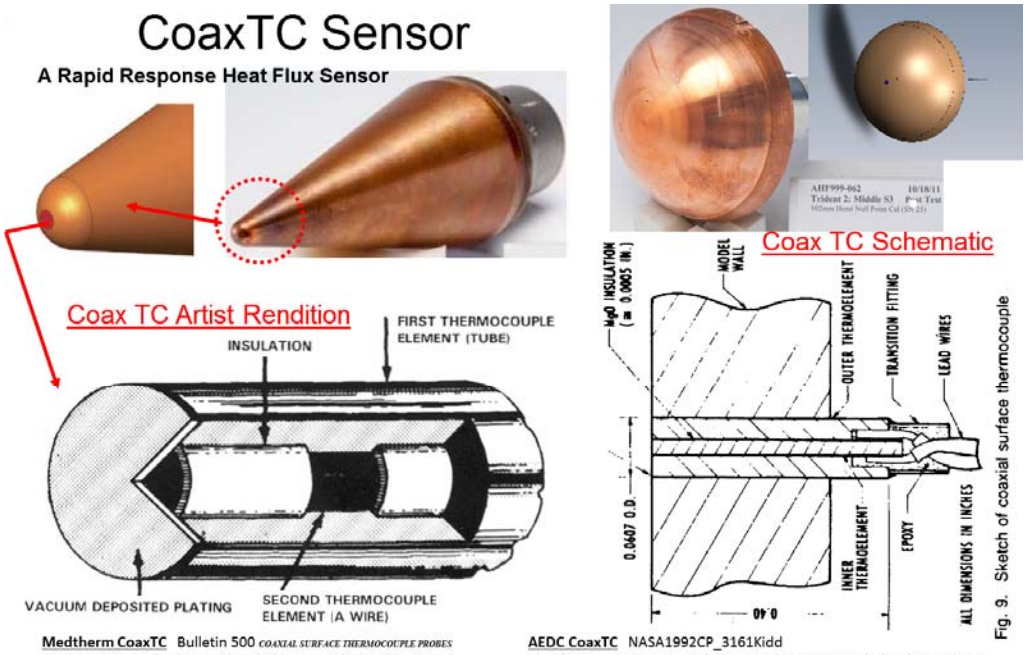

Fig. 9. Sketch of coaxial surface thermocouple

Fig. 2 Coaxial TC sensor schematics and examples of them mounted in Calorimeter bodies

A number of different size and shaped calorimeter bodies (used to house the sensors) were designed and fabricated at NASA Ames. The calorimeter body shapes that are most frequently used are shown in Fig. 3. Each has a spherical nose and a shell thickness at the nose of 10.16mm (0.400") which is designed to match the length, L, of the sensor (see Fig. 3). Matching the shell thickness to the length of the sensor is useful from an analysis point of view. The sensor was potted (by AEDC) into the calorimeter body with a 25.4μm (0.001") thin layer of adhesive [7] between the sensor and the hole in the calorimeter body.

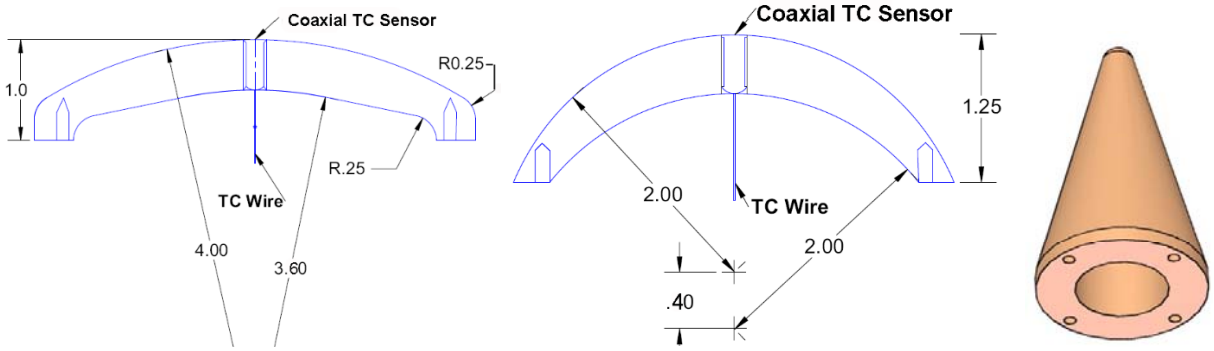

a) 101.6mm diam. IsoQ b) 101.6mm diam. Hemisphere c) 12.7mm diam. sphere cone

Fig. 3 Calorimeter bodies used routinely in the NASA Ames arc jets.

The sensor is not immune to lateral conduction effects as the calorimeter body is in good contact with the sensor through a thin (almost negligible) layer of adhesive. The sensor is predominantly the same material as the calorimeter body and for all practical purposes an integral part of the body. The main issue is with the lateral conduction effects internal to the calorimeter body itself. The question being, how much does lateral conduction affect the surface temperature at the nose of the body?

III. 2D Thermal Conduction Analysis of Calorimeters

To study lateral conduction effects, two-dimensional finite element simulations were performed on the calorimeter body using ANSYS (a commercially available 3D code [8]). Heat flux was imposed on the outer surface of the calorimeter as a boundary condition to ANSYS which then simulates the temperature rise at the nose of the calorimeter as a function of time. The predicted temperature was used as input to a fast running 1D finite element inverse code (used by the arc jets) to deduce the heating at the nose of the calorimeter as a function of time. Differences between the deduced heating from the 1D inverse analysis and the heating imposed in the ANSYS simulation were attributed to lateral conduction effects that are not accounted for in the 1D analysis. These differences are then incorporated into the assessment of uncertainty for each calorimeter. A second effort was directed toward finding a way to correct for 2D lateral conduction effects neglected in the 1D inverse code (used by the arc jets).

A. Finite Slab Analysis

An example of a Finite Slab simulation is shown in Fig. 4. The imposed heat flux is constant with time starting at time t=0. The temperature of the front surface of the slab is the primary quantity of interest from the ANSYS simulation, as that is the temperature is used as input to the 1D finite element inverse heat conduction code which deduces the heat flux as a function of time (necessary to generate the ANSYS simulated surface temperature response). The deduced heat flux from the 1D inverse code reproduces the imposed heat flux, as evidenced by the dashed line hugging the abscissa which is the percent difference between the 1D inverse code heat flux and the heat flux imposed in the ANSYS simulation. This good agreement between the two simulations is verification that both the 1D inverse code and the ANSYS code are consistent with each other. Note that the backside of the slab is modeled as an adiabatic wall by the 1D inverse code and the fidelity of the simulation is maintained long after the heat wave reaches the backside of the slab.

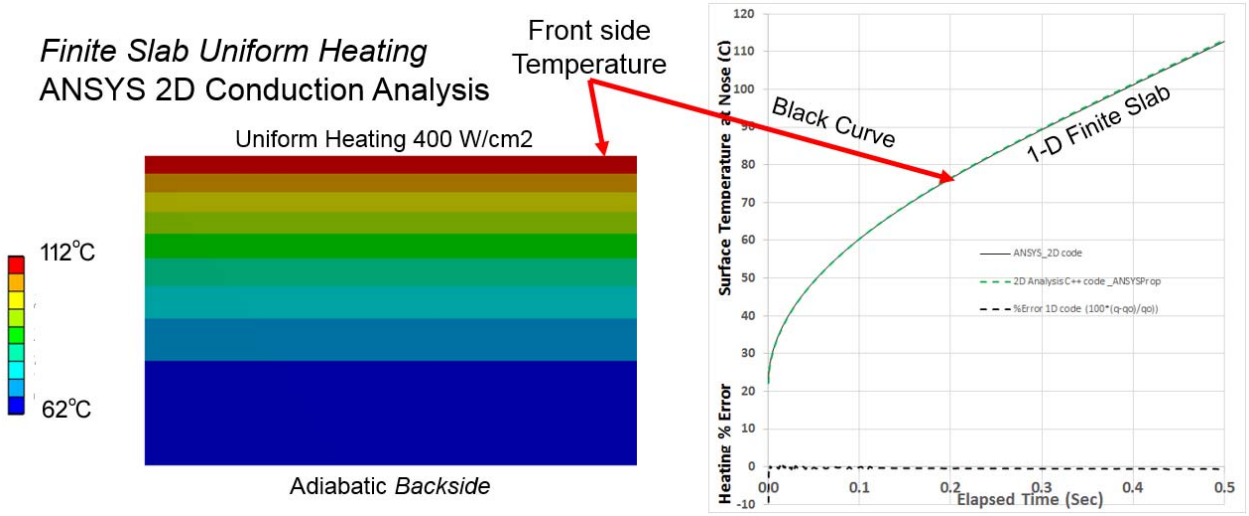

a) Temperature isotherms at t=0.5s b) Temperature history of stagnation point

Fig. 4 Simulation of 1D Finite Slab subjected to uniform heating.

B. Spherical Nose Shaped Body – IsoQ Calorimeter 102mm in diameter

A spherical nose shape is inherently a violation of the 1D assumption in the 1D finite slab inverse analysis. To explore the magnitude of this effect a spherical nose shaped calorimeter known as an IsoQ (Fig. 3a) was investigated. It is assumed that the coaxial Thermocouple is in good thermal contact with the body such that the body and sensor act as single unit. The IsoQ shape experiences a very nearly uniform distribution of aerothermal heating over its outer face (thus the name IsoQ). In the ANSYS simulation uniform heating was imposed over the outer face of the body of the IsoQ calorimeter (see Fig. 5a). During a short exposure (0.5 s) the temperature isotherms follow surfaces of concentric spheres (*r=constant*) across the inner third of the calorimeter (see Fig 5a), much like the model problem of a uniformly heated spherical shell. This is a sufficiently short simulation such that anomalous effects at the corner have not propagated inward toward the nose of the body, and for all practical purposes the central third of the body is acting like a spherical shell with uniform heating. A companion simulation of an actual spherical shell with uniform heating gives the same temperature history (not shown). It will be shown

in section III-C that a 1D inverse analysis (using spherical coordinates) will accurately reproduce the heating rate imposed in the ANSYS simulation.

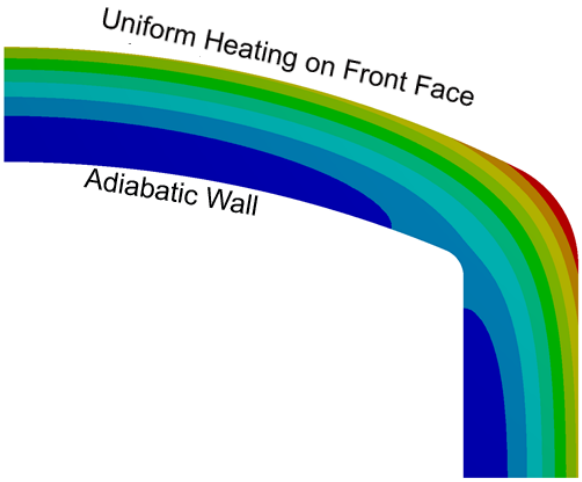

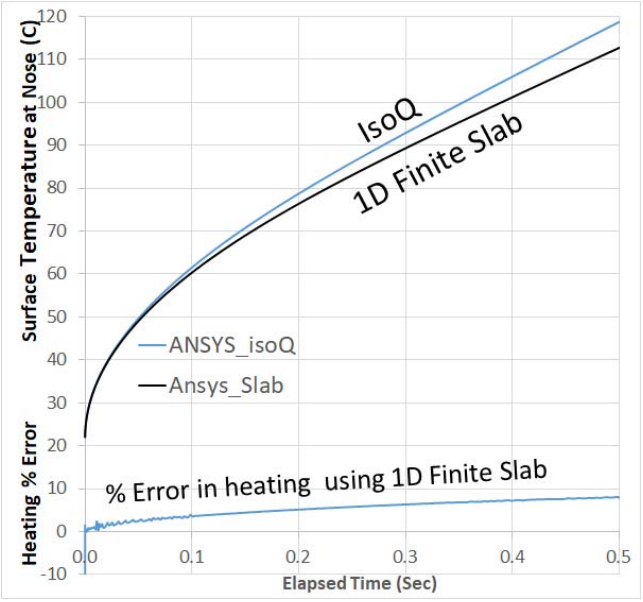

b) Temperature isotherms at t=0.5s b) Temperature history of stagnation point

Fig. 5 ANSYS Simulation of 101.6mm diam. IsoQ body subjected to uniform heating.

The temperature of the IsoQ simulation rises faster than does that of a 1D finite slab. This result, while puzzling at first, can be explained by considering a model problem of a spherical shell which is uniformly heated on its outer surface. The temperature will rise faster on the spherical shell because there is less mass available to absorb heat $\{\text{mass}=\rho\pi 4/3(R_o^3-(R_o-L)^3)=\rho 4\pi R_o^2 L(1-L/R_o+(L/R_o)^2/3\}$ relative to that of an equivalent surface area slab ($\rho 4\pi R_o^2 L$), where R_o is the radius of the sphere and L is the thickness of the shell (or slab).

Now consider a conical slice of the spherical shell with sides that are defined by radial lines emanating from the center of the sphere – note that the conical slice tapers with distance from the surface (see Fig. 6). The conical frustum shape sees no gradients normal to radial lines (isotherms follow surfaces of concentric spheres) and the side of the conical frustum can be treated as an adiabatic wall. An analysis of the conical frustum like shape, with adiabatic side wall, is equivalent to analyzing the full spherical shell where temperature only varies with distance along the radial and with time. Again, the conical slice of material has less areal mass than an equivalent surface area cylindrical slice of material so the temperature will rise more quickly in the case of the conical slice of material (from spherical shell) than it will in the case of the cylindrical slice (from planar finite slab of same thickness). As a result, the planar 1D finite slab inverse code, applied to the temperature history of the conical slice, will over-estimate the heating experienced at the nose of the calorimeter body (see blue line near abscissa).

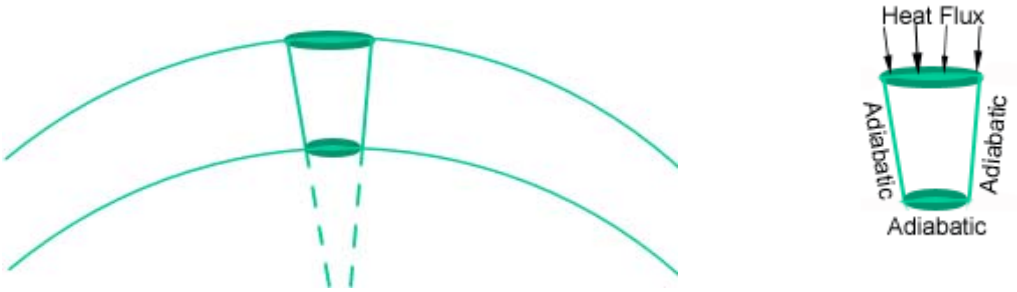

Fig. 6 Schematic of a Spherical shell with a differential slice that is conical in shape

C. Modified 1D Inverse Analysis

To accommodate the spherical effect issue with the 1D inverse analysis, the 1D finite slab code is modified to solve heat transfer to a conical frustum like shape (see Fig. 6b), which involves solving the problem in spherical coordinates (Eq 1.). Keep in mind that the only variation in temperature is in the radial direction by virtue of the sides of frustum being adiabatic.

$$\rho C_p R^2 \frac{\partial T}{\partial t} = k \frac{\partial}{\partial x}\left\{R^2 \frac{\partial T}{\partial x}\right\} \qquad \text{Eq 1}$$

The modified 1D inverse analysis (spherical coordinates) involves dividing up the conical shape into numerous differential elements (see Fig. 7) that are each tapered such that the area of the inner face of the differential element is smaller in area (πR_{k+1}^2) than that of the outer face of the differential element (πR_{k-1}^2), where $R_k = R_o - x_k$.

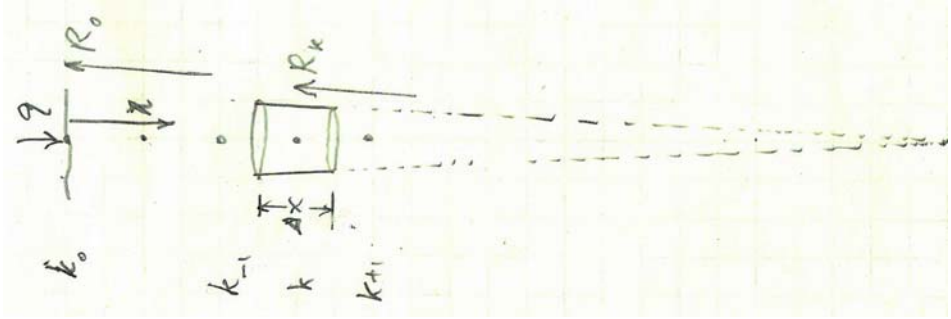

Fig. 7 Schematic of differential slice of conical shape.

Equation 1 can be discretized into equally spaced (∆x) finite elements as follows

$$R_k^2 \rho C_p \frac{T_k^{n+1} - T_k^n}{\Delta t} = k\left\{R_{k+\frac{1}{2}}^2 \frac{T_{k+1}^{n+1} - T_k^{n+1}}{\Delta x} - R_{k-\frac{1}{2}}^2 \frac{T_k^{n+1} - T_{k-1}^{n+1}}{\Delta x}\right\} / \Delta x$$

Where index k is the number of the spatial element, and index n is the time step, $t+n\Delta t$. Setting $\alpha = k/\rho C_p$ and rearranging terms

$$\frac{\Delta x^2}{\alpha \Delta t}\left(T_k^{n+1} - T_k^n\right) = \left(\frac{R_{k+1/2}}{R_k}\right)^2 T_{k+1}^{n+1} - \left(\frac{R_{k-\frac{1}{2}}^2 + R_{k+\frac{1}{2}}^2}{R_k^2}\right) T_k^{n+1} + \left(\frac{R_{k-1/2}}{R_k}\right)^2 T_{k-1}^{n+1}$$

Regrouping terms of like temperature, $T_k^n, T_{k+1}^{n+1}, T_k^{n+1}, T_{k-1}^{n+1}$, gives

$$-\left(\frac{R_{k+1/2}}{R_k}\right)^2 T_{k+1}^{n+1} + \left\{\left(\frac{R_{k-\frac{1}{2}}^2 + R_{k+\frac{1}{2}}^2}{R_k^2}\right) + \frac{\Delta x^2}{\alpha \Delta t}\right\} T_k^{n+1} - \left(\frac{R_{k-\frac{1}{2}}}{R_k}\right)^2 T_{k-1}^{n+1} = \frac{\Delta x^2}{\alpha \Delta t} T_k^n \qquad \text{Eq 2}$$

A B C D

The terms, labeled A, B, C, and D, are the coefficients used in the tri-diagonal solver which are used to invert the matrix needed for a solution to the system of equations. In the case of a cylindrical differential element ($R_o \rightarrow \infty$) the coefficients A, B, C revert back to the values associated with the typical 1D planar finite slab analysis (–1, ($2+\Delta x^2/\alpha dt$), –1 respectively). When the 1D inverse solver is modified in this way, the resulting heat flux deduced by the solver gives back exactly the heat flux imposed in the ANSYS simulation (400 W/cm^2), see blue dashed line in Fig. 8. The excellent match in heating between the ANSYS solver and the modified inverse solver is encouraging.

This analysis is more about spherical shells, than it is about coaxial TC sensors. Keep in mind that the sensor itself is not physically a conical shape. Instead the idea is to solve the heat conduction problem on a sensor/body configuration that is spherical in shape for which a conical frustum like shape is the quasi 1D equivalent. For the remainder of this paper the spherical shell analysis will be referred to as a conical shape analysis in which $R_{conic}=R_{sphere}$. The 1D finite slab inverse analysis will occasionally be referred to as a cylindrical shape analysis ($R_{conic}=\infty$).

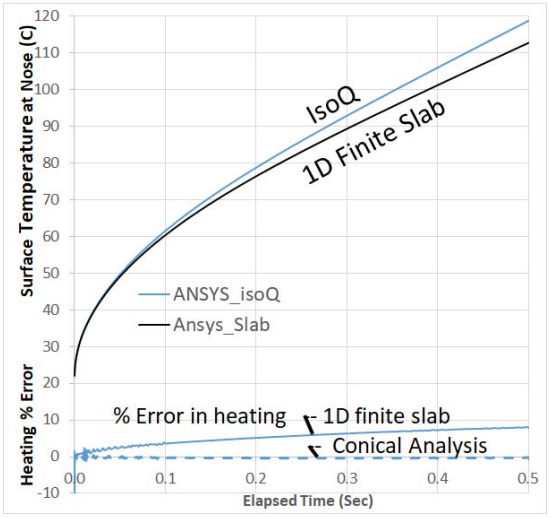

Fig. 8 Percent difference in heat rate between the modified 1D inverse analysis and that which is imposed in ANSYS

D. Non-Uniform Heating Effects

The 2D effects associated with being a spherical body shape is not the only source of uncertainty for the 1D finite slab inverse analysis. According to CFD there is non-uniform heating across the face of the IsoQ calorimeter. That is to say that the IsoQ does not live up to its name, and heat transfer drops off with distance from the centerline of the body.

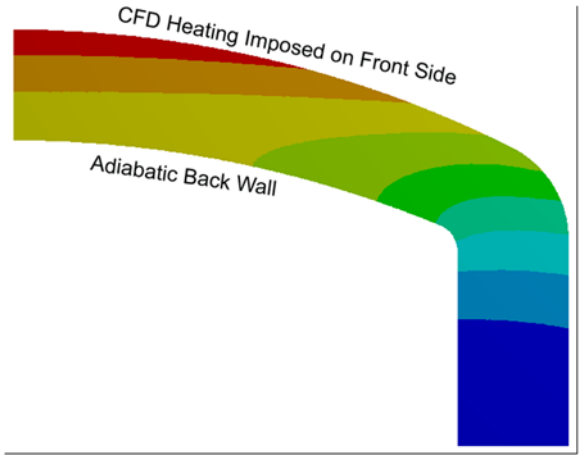

a) Temperature isotherms at t=0.5s

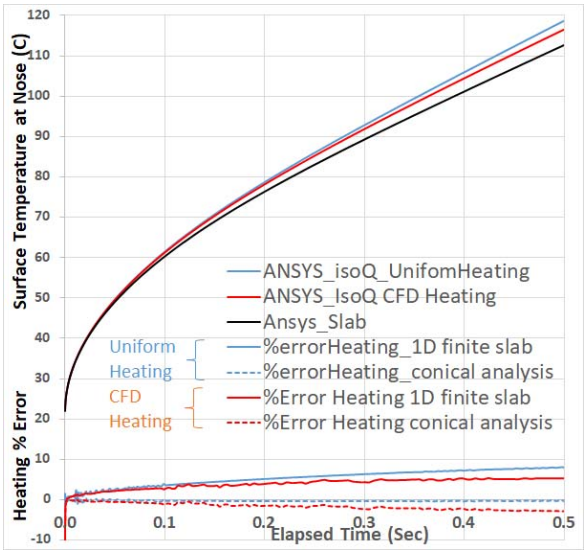

b) Temperature history of stagnation point

Fig. 9 Simulations of the 101.6mm IsoQ with a CFD distribution of heating imposed on its face

The ANSYS predicted temperature at the nose of the "IsoQ" rises more slowly with time when the CFD heating distribution is applied (relative to the simulation with uniform heating). This is attributed to 2D effects associated with lateral cooling (of the centerline) by conduction to the colder outer rim of the body (where heating is lower). Consequently, using the modified 1D spherical shell inverse analysis (aka conical shape analysis) results in an underestimate of the heating levels at the nose of the calorimeter – albeit less of an error than would have been the case with the original 1D finite slab inverse analysis. It is apparent that the non-uniform heating effect is to some extent helping to offset the spherical effects, allowing the 1D finite slab inverse analysis code to give reasonably accurate deduced heating even without modification.

E. Hemispherical Calorimeter (102 mm Diameter)

As calorimeters with smaller spherical nose radii are considered the effects of spherical body and of non-uniform spatial heating become larger. Consider the 102mm diameter Hemispherical calorimeter in which the heating rate imposed on its face diminishes with distance from the centerline (according to *cos(Θ)*). Here the thickness of the body at the nose is a larger fraction of the nose radius than it was for the IsoQ calorimeter (see Fig. 10).

When a 1D finite slab inverse analysis is applied to the temperature (simulated by ANSYS) the 1D code over-estimates the heating by as much as 14%. When a modified version of the code (conical shape) is run there is an under-estimate of the heating at the nose of the calorimeter. Note that this simulation was run for 2 seconds, and that most exposure durations are on the order of ½ seconds, in which case the conical shape version of the code is the better choice.

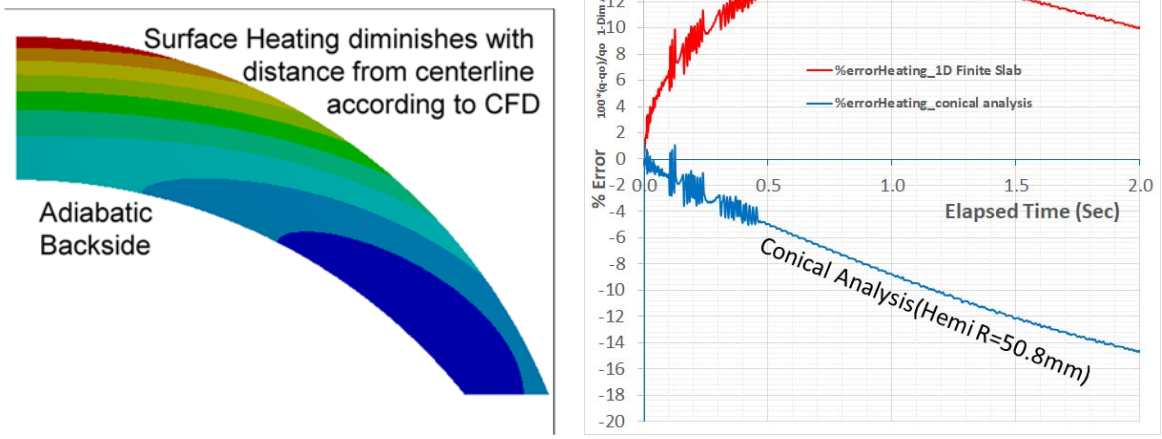

a) Temperature isotherms at t=0.5s b) Error in deduced heating at the stagnation point

Fig. 10 2D conduction simulation of a 101.6mm hemisphere compared to calculations by the 1D inverse code

F. Sphere Cone Calorimeter (12.7 mm diameter)

The most severe case of a small nose radius calorimeter is the 12.7mm diameter sphere cone calorimeter (Fig. 11). The initial temperature rise is faster than that of 1D Slab, due to the usual spherical body effects. At t>0.3s the temperature rises more slowly due to conduction to colder side walls and aft-body. The heat flux deduced by 1D inverse finite slab code is not as far off from the imposed heating as one might have imagined. Deduced heat flux is at most 15% higher than the imposed heat flux (of the ANSYS simulation). Spherical geometry effects appear to be balanced to some extent by the lateral conduction (to the cooler side walls). The conical analysis breaks down (and is not shown here) since nose radius (6.35mm) is smaller than the sensor length (10.16mm). This 1D finite slab analysis is not too bad considering the two effects (spherical nose and non-uniform heating) are huge by themselves, but fortuitously nearly cancel each other in the early stages of exposure (0.1<t<0.6 s).

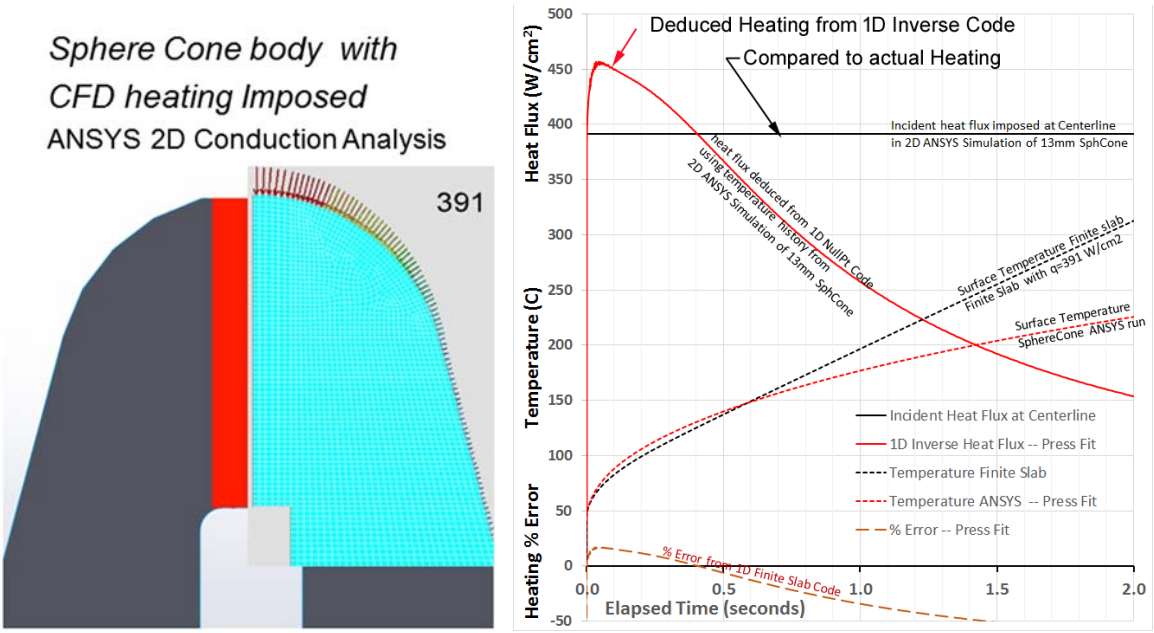

a) Geometry and surface heating distribution b) Temperature history and deduced heating at stagnation point

Fig. 11 Sphere Cone Calorimeter (12.7mm diam.) 2D simulations compared to 1D inverse code

G. Sphere Cone Calorimeter with Adhesive

AEDC began gluing coaxial TC's into the body in 1994 [7] in the interest of electrical insulating the sensor from the body. This was done to eliminate electrical conduction between the dissimilar metals of the sensor and the body into which it was pressed – effectively modifying the thermocouple response. Fortuitously, the adhesive not only acts as an electrical insulator, but it also acts as a thermal insulator to some extent. How does insulating the sensor from the body affect the lateral conduction?

ANSYS was used to simulate the case where a 51 μm (0.002") thick ceramic insulating layer was sandwiched between the sensing element and the calorimeter body (see Fig. 12). The adhesive was made to be twice as thick as its actual thickness in the interest of seeing what is possible if the sensor were more aggressively insulated from the body. Here the adhesive conductivity, density and heat capacity are assumed to be $k=0.7$ *W/(m-K)*, $\rho= 1560$ *kg/m*^{3}, and $C_p=880$ *J/(kg-K)*, respectively. The results with insulation are shown in Fig. 12.

The ANSYS predicted temperature rise at the nose of body is somewhat closer to that of a 1D finite slab analysis as a result of the sensor being slightly more insulated from the body (by virtue of the adhesive). Lateral conduction through the adhesive is never-the-less substantial, and after ½ second of exposure the lateral conduction (to the cold aft-body) again overwhelms the conduction process.

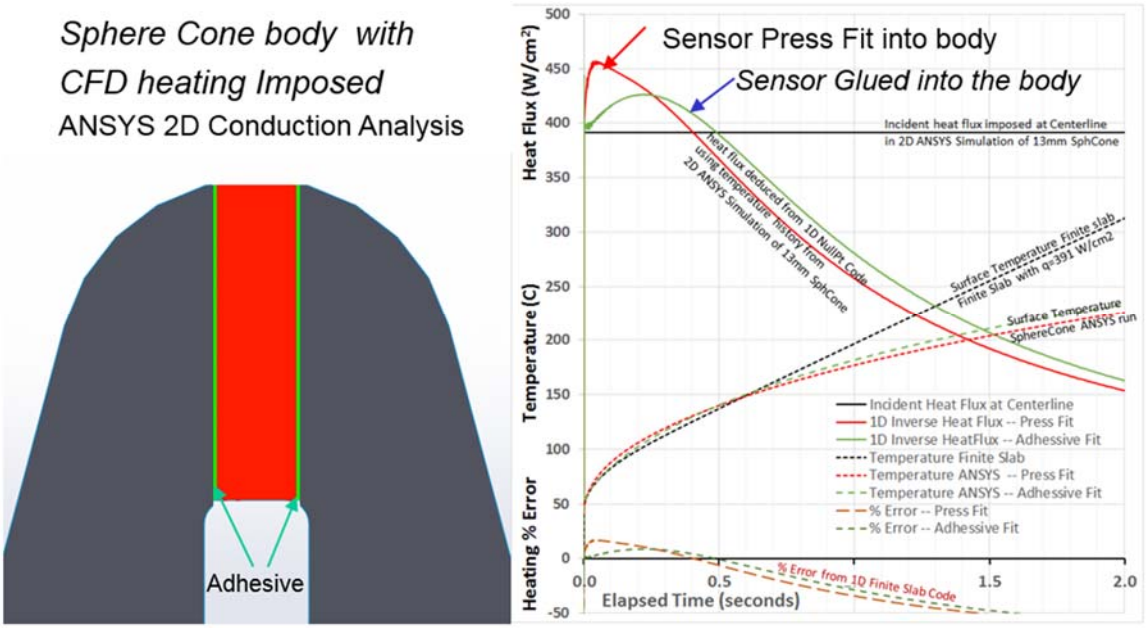

a) Geometry and surface heating distribution b) Temperature history and deduced heating at stagnation point

Fig. 12 Sphere Cone Calorimeter (12.7mm diam.) simulations with adhesive layer between the sensor and the body.

IV. Attempts to Correct the 1D Inverse Analysis

If possible, it would be nice to develop a correction that could be applied to the 1D inverse finite element analysis, so that the stated level of uncertainty could be reduced.

A. Ad hoc Correction

For the most part the two estimates of heating by the 1D inverse analysis code (finite slab and conical frustum shape) seem to straddle the truth (Figs 9 & 10). An ad hoc modification to the conical frustum shape version of the code was investigated, one in which the spherical nose radius of the body was declared to be greater than the actual nose radius. In so doing the modified 1D inverse analysis would hopefully give better agreement with the ANSYS simulation.

In the case of the 101.6 mm diam. IsoQ, the error in the modified 1D inverse analysis is diminished by adopting a nose radius that is twice that of the actual nose radius (see Fig. 13).

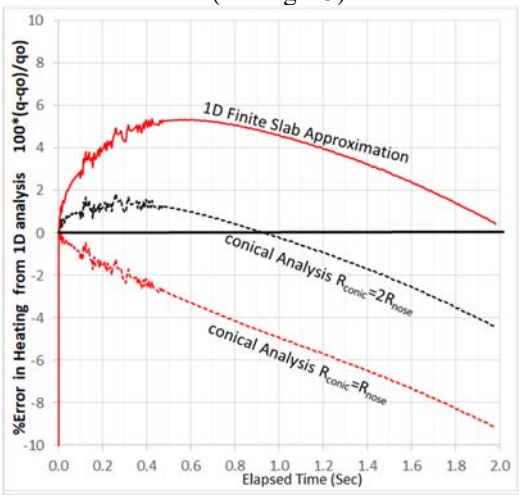

Fig. 13 Error in heating on a 101.6mm diam. IsoQ body using a modified 1D inverse analysis simulation (black line).

While this ad hoc correction doesn't entirely solve the problem, it does offer a step in the right direction toward reducing the error due to lateral heat transfer effects. Notice that these simulations are run for 2 seconds of exposure

and the accuracy of the modified 1D analysis is not bad (especially in the first 1 second of exposure). After 2 seconds of exposure, all 1D analysis is under-estimating the heat flux at the nose of the calorimeter, due to conduction loss to the colder outer rim of the body (where aerothermal heating is lower and near zero on the side the body).

The 101.6mm diameter hemispherical calorimeter was considered next, where lateral cooling (via conduction) to the colder outer rim of the body is more severe. A similar ad hoc correction (declaring nose radius to be twice the actual nose radius) helps to improve the accuracy of the 1D spherical inverse analysis. In so doing the error is greatly reduced in the first 1 second of exposure.

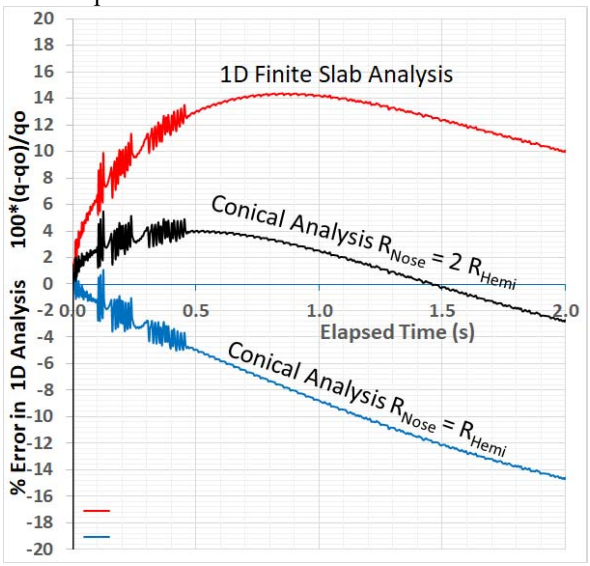

Fig. 14 Error in deduced heating from 1D inverse analysis applied to a 101.6mm diam. Hemispherical body

B. Other Possible Approaches to Modifying the 1D Inverse Analysis

While the results of 1D inverse analysis look promising there is still enough error associated with the 1D finite element analysis that it is worth looking for a better method of correcting the result. A more physics-based correction would be desirable, but the challenge is to come up with a simple enough quasi 1D model that can run quickly (preferably in real time while the arc jet is running) and also be accurate.

The conical modification to the 1D finite element analysis code is easily implemented and is completely general to any axisymmetric shape of interest. All the calorimeter probe body shapes experience spherical effects initially, and later in the exposure the centerline feels the effects of the colder side walls and aft-body (due to lower heating on the sides and back of the body). To accommodate both effects, further modifications to the effective shape of the conical frustum are considered. That is to say analyze an effective shape that is tapered at the top (to accommodate the spherical effects that are felt initially), and longer at the back (and possibly fatter) to emulate the effects of a cold aft-body (see Fig. 15c).

a) 1D Finite Slab. b) Conical Frustum c) longer Conical Frustum

Fig. 15 Possibilities for modeling the spherical shell with alternative quasi 1D shapes

None of the above modifications are difficult to implement, and one could make the argument that the longer aft-body is an elegant (and more physical) way of mimicking the effects of the cold aft-body.

To illustrate the benefit of adopting a modified effective shape for the heat transfer model a 101.6mm diameter hemispherical probe is considered. The original 1D finite slab analysis is shown in red, and the conical shape analysis ($R_{conic} = R_{nose}$) is shown as blue curve (see Fig. 16). Also shown in Fig. 16 (black line) is an analysis using a shape of the type shown in Fig. 15c which is prescribed to be a conic frustum that has $R_{conic} = 1.25*R_{ActualNose}$ and

is also 10% longer than the actual spherical shell is thick. This adaptation to the shape helps to more accurately reproduce the imposed heating rate in the early stages of exposure ($0< t <0.5$ s) while maintaining a relatively accurate measure of heating in the later stages of exposure ($0.5< t < 1.5$ s).

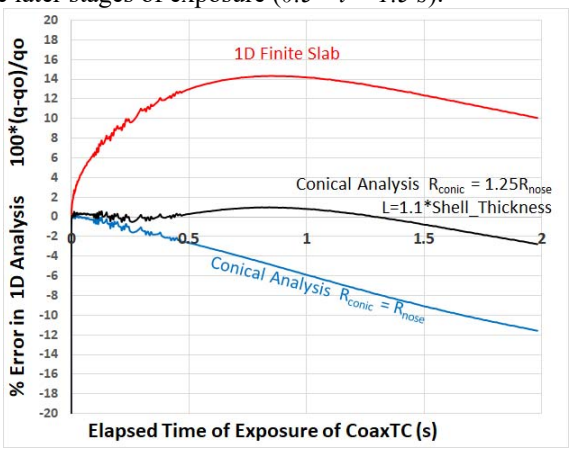

Fig. 16 Error in deduced heating from 1D inverse analysis using a modified 1D analysis

C. Time variation in heating effects on accuracy

One of the main benefits of the coaxial Thermocouple is its ability to sense fast changes in the heating distribution, associated with rapidly sweeping the calorimeter through the flow. An additional simulation of the IsoQ was performed, one in which the heating was ramped up and down according to $cos(t\pi)$ while at the same time maintaining a realistic radial distribution of heating (from CFD) over the face of the IsoQ (see black line in Fig. 17a). As expected the finite slab analysis over-estimates the heat rate deduced from the temperature history produced by ANSYS (surface temperature measured by coaxial TC), see the red curve.

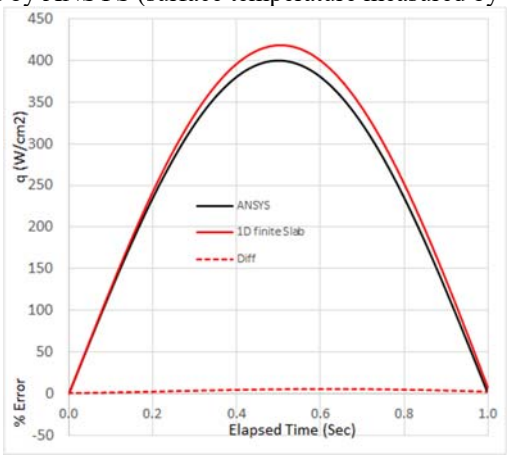

a) Heat rate prescribed in ANSYS and deduced by 1D finite slab

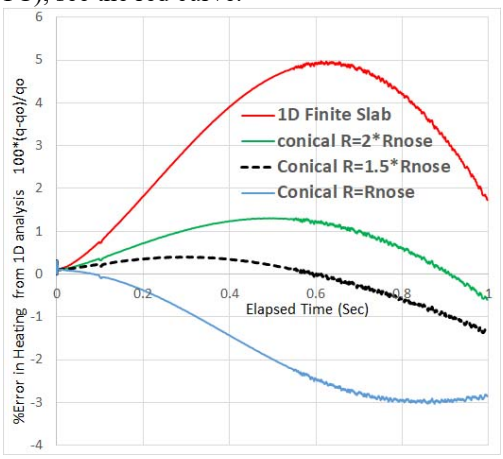

b) %error in 1D analysis

Fig. 17 Response of modified 1D analysis to a time varying heating rate on the 102mm hemispherical calorimeter.

The percent error between the 1D inverse analysis and the exact heating imposed on the ANSYS simulation is shown in Fig. 17b. Here a conical shaped model $R_{conic} = R_{noseISOQ}$ is shown in blue. Also shown are conical models associated with larger spherical bodies, $R_{conic} = 2R_{noseISOQ}$ (shown in green), and $R_{conic} = 1.5R_{noseISOQ}$ (shown in black). The conical model whose $R_{conic} = 1.5R_{noseISOQ}$ gives a reasonably good reproduction of the exact heating rate.

In practice the calorimeters are swept rapidly across the jet, thus finishing the traverse in less than ½ second. For example three calorimeters were mounted on a three pronged probe holder at a location 76mm downstream of the NASA Ames IHF 229mm nozzle; the sweep speed was 0.75m/s. The heat flux measured by the coaxial TC probe (red and blue lines) and the Gardon gauge probe (black line) are shown in Fig. 18. The coaxial TC probe is analyzed in two ways: 1) traditional 1D finite slab analysis (blue dotted line) and 2) a 1D analysis using the conic frustum shape described in section IV-B ($R_{conic} = 1.25*R_{ActualNose}$ L=1.1*Shell-Thickness) shown in red. The analysis using the conic frustum model gives slightly lower heating than the traditional 1D finite slab analysis (as expected). The slightly lower heating deduced by the coaxial TC produces better agreements with the Gardon gauge

probe (black line). Also, the conic analysis gives better agreement between the forward and backward sweeps of the coaxial TC, and the deduced heating after the backward sweep ($|r|>175mm$) is more nearly zero (as it should be). While this is not proof of higher accuracy on the part of a conic analysis, it is encouraging to see. Figure 18 also shows the heat flux measured by a slug calorimeter (orange circle) indicating higher heating than either the coaxial TC or the Gardon gauge. The reason for this discrepancy is not known, but, perhaps the slug is not actually on centerline; it would not need to be off centerline by much (1.5cm) in order to explain this difference.

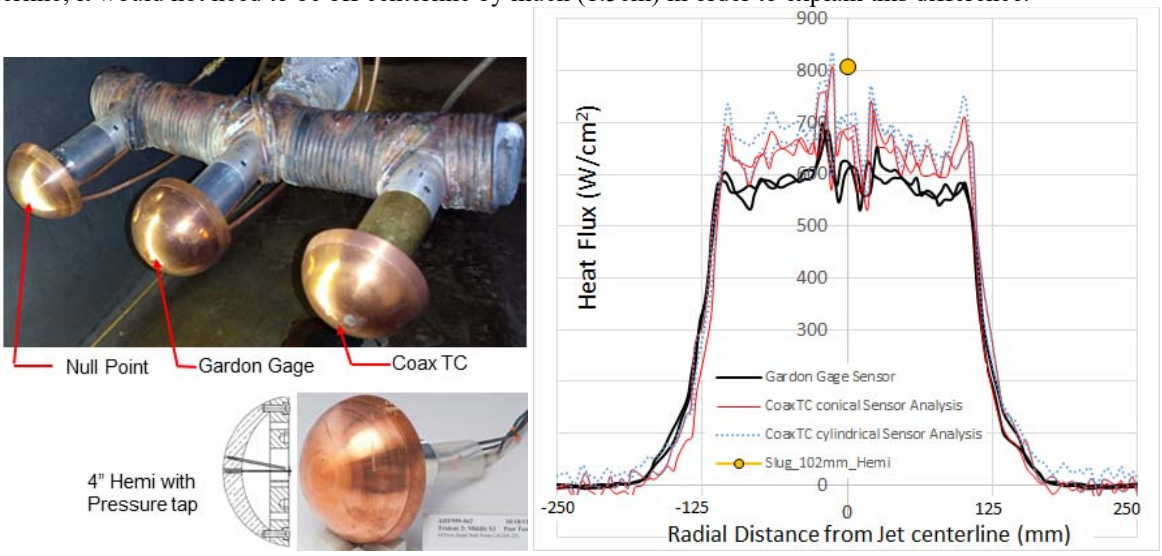

Fig. 18 Comparison of heat flux measurements of the IHF229mm nozzle at moderate conditions by 3 different sensors

Here the shape of the heating distribution is desired in the interest of obtaining the ratio of centerline enthalpy to the average (or bulk) enthalpy. The value of having multiple different sensors measuring the same conditions cannot be understated. If there were only one measurement it may have concluded that noise was responsible for the local minima and maxima in heating distribution in the neighborhood of the centerline. But when the same response is obtained with two drastically different instruments, one is lead to believe the local minima and maxima are real and in this case due to standing waves in the nozzle.

V. Conclusions

Recent introduction of coaxial Thermocouple type calorimeters into the NASA Ames arc jet facilities has inspired an analysis of 2D conduction effects associated with this type of calorimeter. The 1D finite slab inverse analysis (which is typically used to deduce the heat transfer to the calorimeter) relies on the assumption that lateral conduction (i.e., 2D effects) is negligible. The ANSYS finite element solver was used to develop accurate simulations of the calorimeter's temperature distribution as a function of time. These simulations were used to provide surface temperature data that could be used as input to the 1D inverse finite element solver which is used to deduce heat flux. The 1D inverse solver relies on the assumption that lateral heating effects are negligible.

These simulations found that all calorimeters suffer lateral conduction effects to some extent and that the lateral conduction is due to two effects; 1) curved nose shape effect causing the internal heating to behave like that of a spherical shell (rather than 1D planar finite slab) and 2) the non-uniform surface heating distribution effect that leads to lateral conduction losses to the colder off-centerline region of the calorimeter (for the calorimeters studied here).

For the large nose radius calorimeters the lateral conduction effects are relatively small, relative to other possible sources of error. However, for small nose radius calorimeter probes the lateral conduction effects can be large due to the spherical shell being thick relative to the nose radius of the body.

The effects of adhesive acting as a thermal insulator between the sensing element and the body were investigated and found to be small and not significantly different from the case where the sensor makes a press fit with the body.

Corrections to the 1D inverse solver were pursued and the most compelling correction involved treating the heat transfer model as a conical frustum like shape rather than a 1D finite slab. Modifying the 1D inverse finite element code to solve for a conical shape rather than a finite slab improved the deduced heating from the 1D code. But this modification did not correct for the effects of non-uniform heating across the face of the calorimeter. An ad hoc correction was suggested in which the nose radius of the calorimeter was declared (in the modified 1D code) to be larger than the actual nose radius of the probe. This correction brought the heat flux deduced from the 1D code to

within a few percent of the actual heat flux. Furthermore, declaring the spherical shell to be 10% thicker than the actual shell thickness helped to accommodate the effects associated with non-uniform surface heating which leads to lateral conduction losses to the colder off-centerline region of the calorimeter. These modifications to the heat transfer model (conical frustum like shape and shell thicker than actual) can be tuned for each of the various calorimeter bodies (size and shape) to obtain a more optimal response by the 1D finite element analysis code. While the corrections are not perfect, the resulting determination of heat transfer is potentially more accurate than that which is obtained when using the planar 1D finite slab assumption.

Acknowledgments

We would like to thank Joe Harman, Tahir Gökçen, Dinesh Prabhu, Kristina Skokova, and Megan McDonald for helpful conversations. And also special thanks to Medtherm and the AEDC sensors group for providing coaxial TCs in the NASA Ames calorimeters. This work was funded under the NASA Strategic Capabilities Assets Program (SCAP).

References

[1] "ASTM Standard E457-96; Standard Test Method for Measuring Heat-Transfer Rate Using a Thermal Capacitance (Slug) Calorimeter," ASTM International, West Conshohocken, PA, http://www.astm.org, 2002, 2002.

[2] R. Gardon, "ASTM Standard E511-07 Standard Test Method for Measuring Heat Flux Using a Copper-Constantan Circular Foil, Heat-Flux Transducer," ASTM International, http://www.astm.org, West Conshohocken, PA, 2007.

[3] "ASTM Standard E598-96; Standard Test Method for Measuring Heat-Transfer Rates from High-Energy Environments Using a Transient Null-Point Calorimeter," ASTM International, West Conshohocken, PA, http://www.astm.org, 2002.

[4] C. T. Kidd, "High Heat-Flux Measurements and Experimental Calibrations/Characterizations," in *NASA CP 3061*, NASA Langley Measurement Technology Conference: pp. 317-335, 1993.

[5] Medtherm Corp, "Coaxial Surface Thermocouple Probe, Bulletin 500," Medtherm Corp., , PO Box 412 Huntsville AL 35804, Ph 256-837-2000.

[6] F. Kreith, Principles of Heat Transfer, New York: Intext Press, Inc. pp 204-206, 1973.

[7] C. T. Kidd, C. G. Nelson and W. T. and Scott, "Extraneous Thermoelectric EMF Effects Resulting from the Press-Fit Installation of Coaxial Surface Thermocouples in Metal Models," in *Proceedings of the 40th International Instrumentation Symposium*, Instrument Society of America, Research Triangle Park, NC, pp. 317-335, 1994.

[8] ANSYS, "Engineering Simulation & 3-D Design Software | ANSYS," ANSYS, [Online]. Available: http://www.ansys.com/.